JOURNAL OF THERMAL STRESSES
https://doi.org/10.1080/01495739.2022.2155742

Temperature effects on microcracks and elastic wave velocities in carbonates

Hui Qi[a], Jing Ba[a], and José M. Carcione[a,b]

[a]School of Earth Sciences and Engineering, Hohai University, Nanjing, China; [b]National Institute of Oceanography and Applied Geophysics – OGS, Trieste, Italy

ABSTRACT

We investigate the effect of temperature on the elastic properties of rocks by combining the thermal-damage factor (TDF) with the Gassmann equation. The resulting model is tested in carbonate samples by analyzing the ultrasonic wave velocity. A comparison between the estimated and measured TDF shows that the model quantitatively describes the behavior of carbonates at relatively low temperatures, while the high-temperature one is underestimated. The dry- and wet-rock TDF difference increases significantly with increasing temperature, and the TDF is highly affected by the rock permeability and microcrack aspect ratio.

ARTICLE HISTORY
Received 27 December 2021
Accepted 23 February 2022

KEYWORDS
Fluid; microcracks; porosity; thermal-damage factor; wave velocity

1. Introduction

The effect of temperature has important effects on the exploration and development regarding coal mining, nuclear waste storage, and geothermal and deep hydrocarbon resources [1–4], in particular on rock microstructure [5, 6], and specifically the presence of microcracks, which affect wave velocity and attenuation [7–10].

The effect of high temperature varies with the type of rock [11–15] and many works analyze the thermal damage. Tian et al. [13] found that the bulk density decreases significantly above 500 °C, the porosity increases above 300 °C, and the permeability increases gradually with temperature. The variations of the rock mechanical properties can be quantified with the thermal damage factor (TDF), first proposed by Dougill et al. [16] (see also [17–21]). Zhang et al. [22] performed an experimental study on the thermal-damage characteristics of limestone, showing that the peak compressive strength and elastic modulus decreases, but the peak strain increases. The TDF increases rapidly in the range 200–600 °C.

The rock properties are affected by several factors, namely the fluids, minerals, porosity, permeability and pressure [23, 24], including temperature [25–27]. Moreover, temperature variations affect the microcrack geometry [14]. In this sense, the scanning electron microscopy was used extensively to study the behavior of microcracks at high temperatures [28–31].

In this work, we consider carbonate samples and analyze the critical temperature corresponding to the irreversible threshold for microcrack propagation, based on the theory of [32, 33]. First, the experimental setup is illustrated. Then, we estimate the TDFs of dry and saturated rocks, by combining the thermal-damage model with the Gassmann equation [34, 35]. Finally, we analyze the effects on bulk density, permeability and microcrack features.

CONTACT Jing Ba jba@hhu.edu.cn School of Earth Sciences and Engineering, Hohai University, Nanjing, China

2. Experiments

2.1. Carbonate samples

Six light gray carbonate samples are collected from Sichuan Basin, Western China, which are granular dolomites with dissolution pores and a small amount of clay and surface pores developed. The reservoir depth is 6 km, with an *in situ* temperature of approximately 130 °C. The pore structure is complex, consisting of intergranular pores and microcracks (grain contacts). The samples are cylindrical, ranging in diameter from 24.92 to 25.23 mm and lengths from 30.93 to 46.99 mm. Porosity, permeability and ultrasonic measurements are made [36]. The properties are given in Table 1.

2.2. Procedure

The ultrasonic pulse method is used to measure the acoustic wave velocities [37] at 1 MHz. During the test, the temperature is increased by a heating wire in the high-pressure vessel, with an accuracy of 1 °C. In order to analyze the thermal damage of the samples, the initial properties before heating are given in Table 1.

The samples are first dried in an oven for 36 h and then sealed with rubber jackets and placed in a high-pressure vessel. The jacket separates the sample from heated silicone oil. Dry- and wet-rock measurements are carried out at a confining pressure of 80 MPa and temperatures of 20, 40, 60, 80, 100, 110, 115 and 130 °C. On another experiment, the pore pressure is 10 MPa and the confining pressure varies as 15, 20, 25, 30, 40, 50, 60, 70 and 80 MPa for a temperature of 130 °C. Wave velocities are then obtained from the travel times.

2.3. Results

Figure 1 shows that the measured P- and S-wave velocities increase as a function of confining pressure. Figure 2 shows a P- and S-wave velocity crossplot as a function of temperature at dry and water-saturation conditions and 80 MPa confining pressure. When the temperature rises to 130 °C, the P- and S-wet-rock velocities decrease by 2.61% and 3.46% on average, whereas the dry ones decrease by 2.26% and 1.74%, respectively. Thermal damage can be correlated with velocity reduction caused by the effects of the fluid and microcracks.

3. Theory

3.1. Thermal-damage theory

Zhao et al. [38] define the TDF in terms of strain. For elastic media, we have

$$\sigma = E_0 \varepsilon_0 \tag{1}$$

where σ, E_0 and ε_0 denote stress, elastic modulus and strain, respectively, at the undamaged state. When the rock is damaged, the stress–strain is [39]:

Table 1. Properties of the carbonate samples.

Sample number	Porosity (%)	Dry density (g/cm^3)	Water saturated density (g/cm^3)	Permeability (mD)
1	1.41	2.692	2.710	0.068
2	4.26	2.690	2.740	3.441
3	4.44	2.714	2.760	0.241
4	5.93	2.651	2.720	0.963
5	10.37	2.552	2.652	1.800
6	17.35	2.328	2.500	4.151

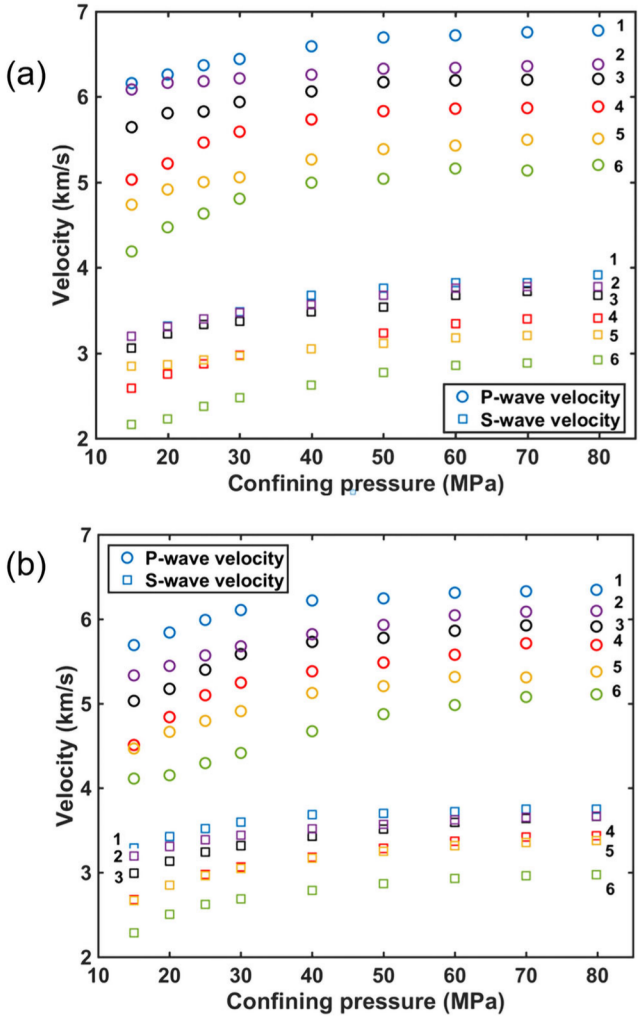

Figure 1. P- and S-wave velocities as a function of the confining pressure at 130 °C for water-saturation (a) and dry (b) conditions.

$$\sigma = E_0(1-D)\varepsilon_1 \tag{2}$$

where $E_T = E_0(1-D)$ represents the damaged elastic modulus and ε_1 represents the related strain. The thermal damage at temperature T is

$$D(T) = 1 - \frac{E_T}{E_0}. \tag{3}$$

Elastic modulus and P-wave velocity are related by

$$E_0 = \frac{\rho_0 V_{P0}^2 (1+\nu_0)(1-2\nu_0)}{1-\nu_0} \tag{4}$$

where ρ_0, V_{P0} and ν_0 are the density, P-wave velocity and Poisson's ratio of the undamaged rock, respectively.

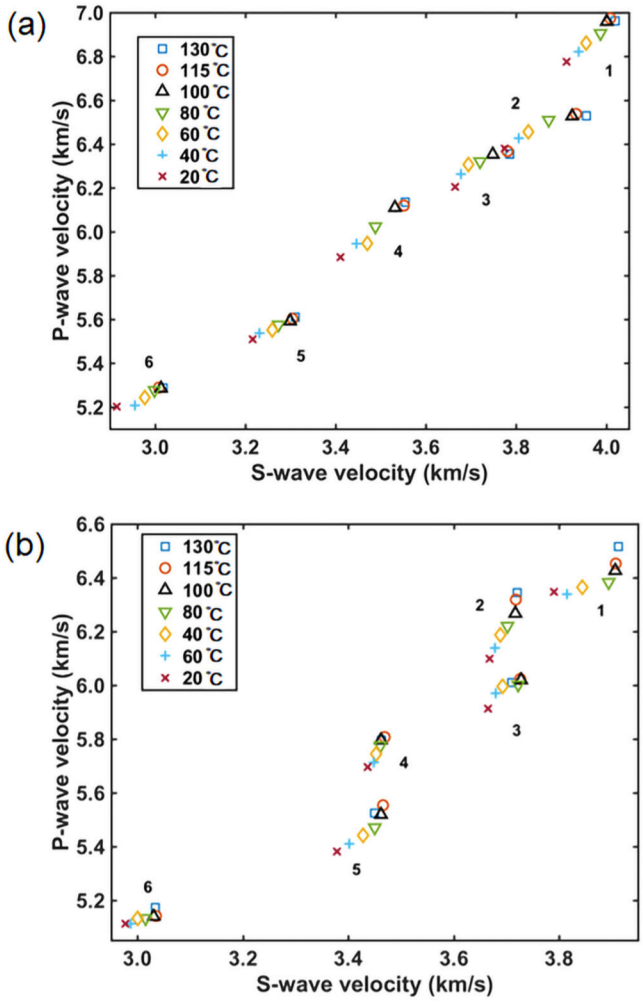

Figure 2. P-wave velocity as a function of the S-wave velocity at different temperatures at water (a) and dry-saturation (b) conditions.

Based on Equations (3) and (4), we obtain

$$D(T) = 1 - \left(\frac{V_{PT}}{V_{P0}}\right)^2 \frac{\rho_T(1+\nu_T)(1-2\nu_T)(1-\nu_0)}{\rho_0(1-\nu_T)(1+\nu_0)(1-2\nu_0)} \tag{5}$$

where ρ_T, V_{PT} and ν_T are the density, P-wave velocity and Poisson's ratio of the damaged rock, respectively.

Temperature is varied from room temperature to 130 °C. The variation of ρ_T and ν_T can be neglected and we have [20, 22, 40]. Equation (6) is applied to analyze the impact of temperature on TDF based on the constant-pressure measurements.

$$D(T) = 1 - \left(\frac{V_{PT}}{V_{P0}}\right)^2. \tag{6}$$

3.2. Model with microcracks

Increasing temperature and rock damage expand the microcracks. According to fracture mechanics [41], when the microcrack expansion force (the stress intensity factor) exceeds a critical value,

there is instability and irreversibility. David and Zimmerman [33] and Vernik and Kachanov [42] report the microcrack porosity

$$\phi_2 = \frac{4\pi\alpha\beta}{3} \tag{7}$$

where β is the microcrack density and α is the aspect ratio.

First, we obtain the ultrasonic experimental data varying with effective pressure at different temperatures. We consider that the microcracks are closed at a high effective pressure, and only stiff pores are present, whose moduli can be estimated from the velocities. The effective bulk and shear moduli as a function of the microcrack density are [43]:

$$K_{\text{eff}} = K_{\text{stiff}} \Big/ \left(1 + \frac{16\left(1 - (\nu_{\text{stiff}})^2\right)\beta}{9(1 - 2\nu_{\text{stiff}})}\right), \tag{8}$$

$$\mu_{\text{eff}} = \mu_{\text{stiff}} \Big/ \left(1 + \frac{32(1 - \nu_{\text{stiff}})(5 - \nu_{\text{stiff}})\beta}{45(2 - \nu_{\text{stiff}})}\right) \tag{9}$$

where $\nu_{\text{stiff}} = (3K_{\text{stiff}} - 2\mu_{\text{stiff}})/(6K_{\text{stiff}} + 2\mu_{\text{stiff}})$ is the Poisson ratio of the stiff pores and K_{stiff} and G_{stiff} are the related moduli. Poisson's ratio and Young's modulus of rock are related to microcrack density [44]. Then, the microcrack density at a given temperature and effective pressure can be obtained by least-square regression based on Equations (8) and (9). The microcrack aspect ratio as a function of the effective pressure p is

$$\alpha = \frac{4\left[1 - (\nu_s)^2\right]p}{\pi E_s} \tag{10}$$

where E_s is Young's modulus at high effective pressures, given by $E_s = 3K_s(1 - \nu_s)$, where ν_s is the Poisson ratio.

On the other hand, the critical temperature corresponding to the irreversible threshold of microcrack propagation proposed by Ravalec and Guéguen [32] is

$$T_c = T_i + (P - p_i)\frac{1}{\alpha_m}\left(\frac{1}{K_f} + \frac{1}{\alpha_0 K_0}\right), \tag{11}$$

$$\alpha_m = \alpha_r - \alpha_f, \tag{12}$$

$$\alpha_b = (1 - \phi)\alpha_s + \phi\alpha_r \tag{13}$$

where α_m, α_r, α_f, α_b and α_s are the fluid mass content changes at constant stress and pressure, the pore thermal expansion coefficient, the fluid thermal expansivity, the bulk thermal expansivity and the mineral thermal expansivity, respectively, K_0 is the dry-rock bulk modulus, ϕ is the porosity, T_c is the critical temperature, T_i is the temperature at a given depth before heating, P is the confining pressure, P_i is the fluid pressure at a given depth before heating and α_0 is the microcrack aspect ratio.

Equation (11) indicates that the critical temperature is mainly controlled the microcrack aspect ratio α_{P0} and the dry-rock bulk modulus K_0, as shown in Figure 3. The temperature is 80 °C, $\alpha_m = -46.2 \times 10^{-5}$ and the range of microcrack aspect ratios is 10^{-2}–10^{-1} [32].

3.3. Thermal-damage estimation

Equation (6) suggests that the key parameter associated with the rock thermal damage is the compressional wave velocity. Based on the velocity equations of the Gassmann theory proposed by Murphy et al. [35], we perform a fluid substitution to estimate the TDF:

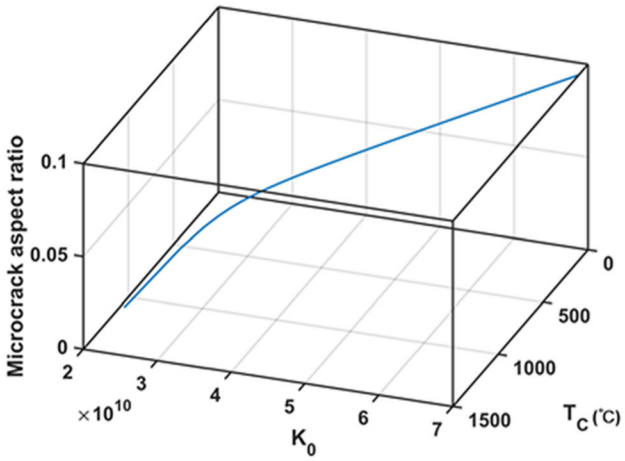

Figure 3. Microcrack aspect ratio as a function of the mineral modulus and critical temperature.

$$\rho_{\text{sat}} V_{P\text{sat}}^2 = K_P + K_{\text{dry}} + \frac{4}{3}\mu, \tag{14}$$

$$\rho_{\text{sat}} V_{S\text{sat}}^2 = \mu, \tag{15}$$

$$K_P = \frac{\left(1 - \frac{K_{\text{dry}}}{K_0}\right)^2}{\frac{\phi}{K_f} + \frac{1-\phi}{K_0} - \frac{K_{\text{dry}}}{K_0^2}} \tag{16}$$

where K_P is the wet-rock pore bulk modulus, K_f is the fluid bulk modulus, K_{dry} is the dry-rock bulk modulus, ρ_{sat} is the wet-rock density, $V_{P\text{sat}}$ and $V_{S\text{sat}}$ are the wet-rock P- and S-wave velocities, respectively, and μ is the shear modulus.

The dry-rock bulk and shear moduli are

$$K_{\text{dry}} = \rho_{\text{dry}} V_{P\text{dry}}^2 - \frac{4}{3}\mu, \tag{17}$$

$$\mu = \rho_{\text{dry}} V_{S\text{dry}}^2 \tag{18}$$

where ρ_{dry} is the dry-rock density, and $V_{P\text{dry}}$ and $V_{S\text{dry}}$ the corresponding P- and S-wave velocities, respectively.

Equation (6) yields the TDF of the dry rock at different temperatures, based on the measured P-wave velocities, and the bulk and shear moduli are obtained from Equations (17) and (18), respectively. The thermal damage of the saturated rock at different temperatures is estimated by using Equations (6) and (14)–(18) as

$$D_{\text{sat}}(T) = D_{\text{dry}}(T) \times \frac{\rho_{\text{dry}} V_{P0\text{dry}}^2}{\rho_{\text{dry}} V_{P0\text{dry}}^2 + K_{P0}} - \frac{K_P - K_{P0}}{\rho_{\text{dry}} V_{P0\text{dry}}^2 + K_{P0}} \tag{19}$$

where K_{P0} is the wet-rock pore bulk modulus at the undamaged state, $D_{\text{sat}}(T)$ and $D_{\text{dry}}(T)$ are the wet- and dry-rock TDFs, respectively, and $V_{P0\text{dry}}$ is the dry-rock compressional wave velocity at the undamaged state.

Based on Equation (19), the wet-rock TDF is obtained from the thermal damage of the dry rock. Figure 4 gives the workflow. The key parameters include the measured dry-rock P-wave velocity and density, and the wet-rock pore bulk modulus. We first estimate the bulk modulus of the rock matrix from the mineral composition. Batzle–Wang equations [45] are used to estimate

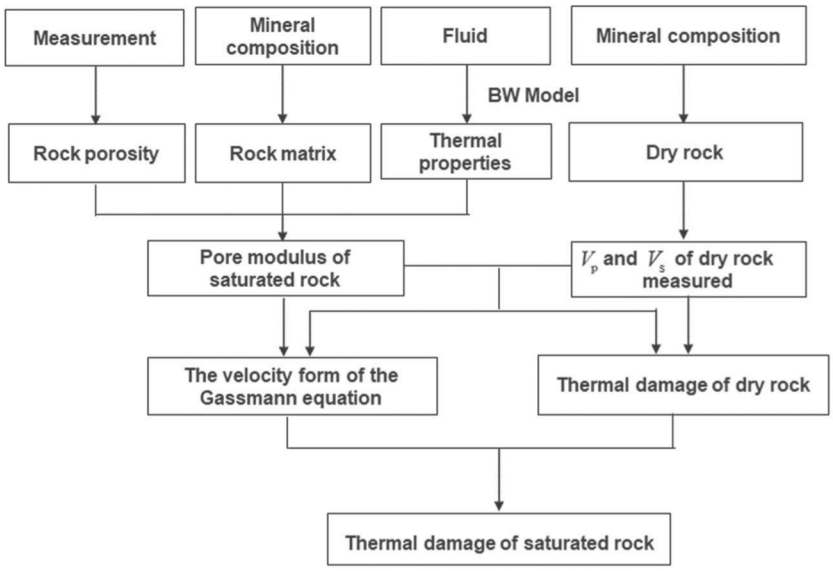

Figure 4. Workflow for estimating the thermal damage of the saturated rock at different temperatures.

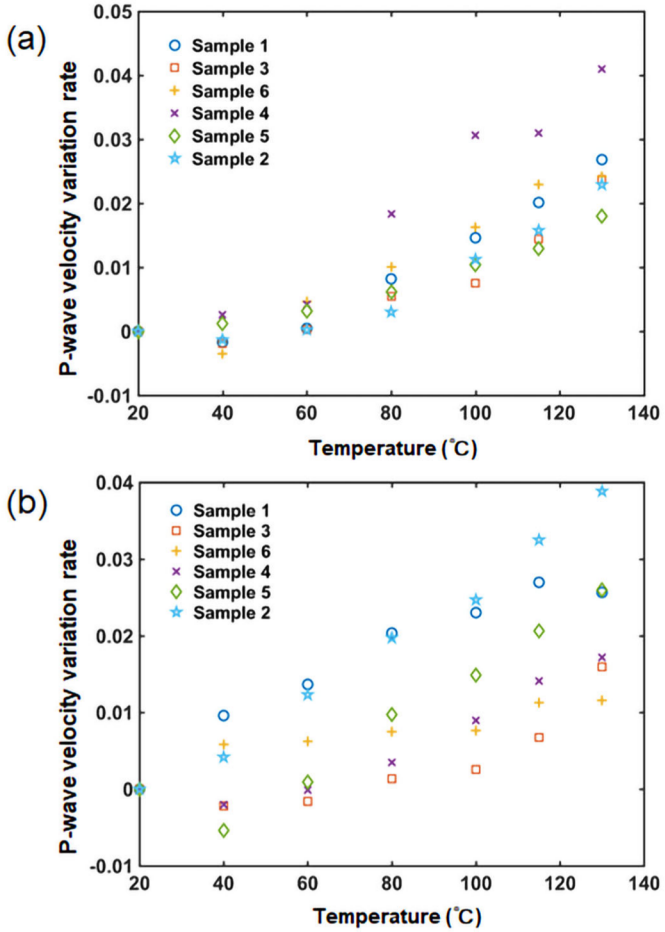

Figure 5. P-wave velocity variation rate as a function of temperature at water-saturation (a) and dry (b) conditions.

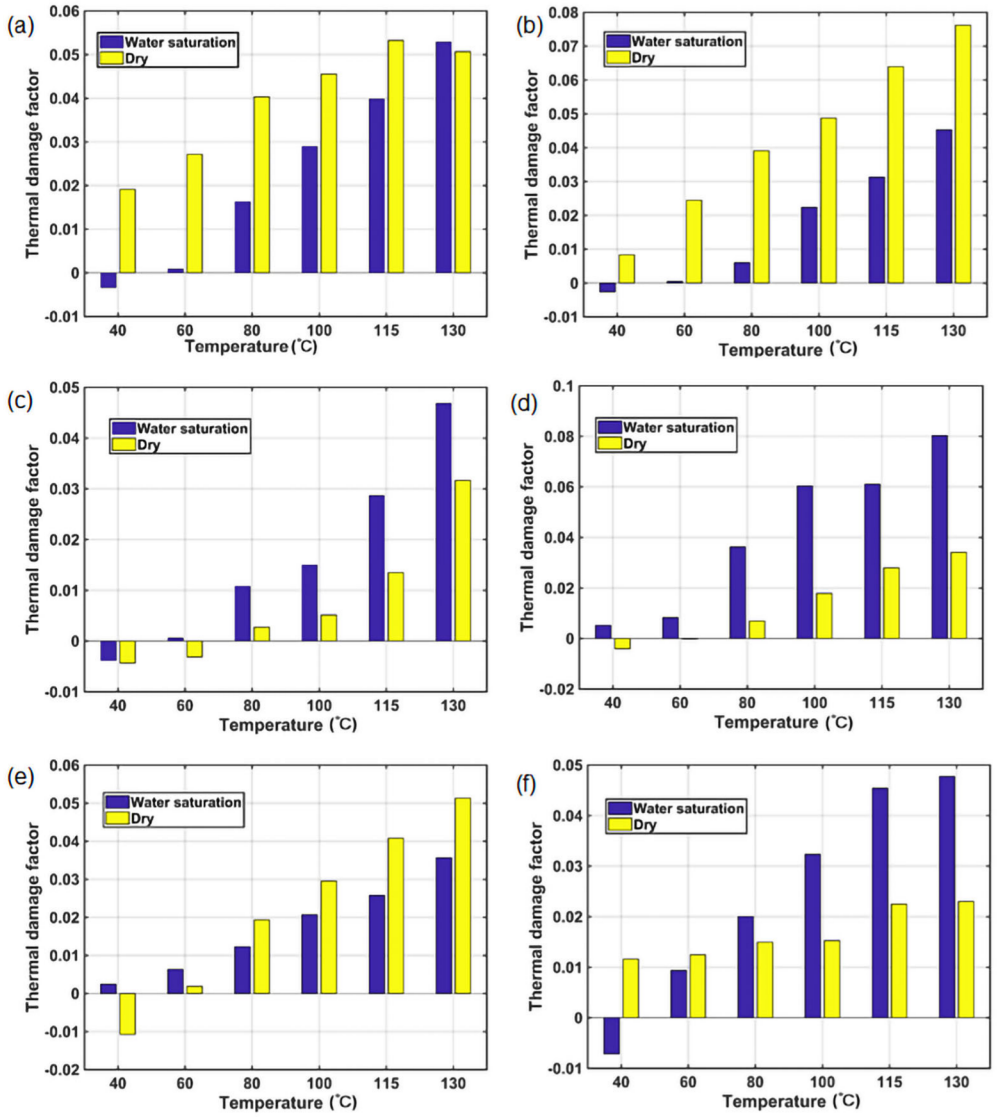

Figure 6. TDF as a function of temperature for (a) sample 1; (b) sample 2; (c) sample 3; (d) sample 4; (e) sample 5; (f) sample 6 at water-saturation and dry conditions.

the properties of the fluid, where the porosity is given in Table 1. These parameters are substituted into Equation (16) to obtain the wet-rock pore bulk modulus of saturated rock at different temperatures.

Based on the measured wet-rock P-wave velocity, the dry-rock thermal damage can be obtained as

$$D_{\mathrm{dry}}(T) = D_{\mathrm{sat}}(T) \times \frac{\rho_{\mathrm{sat}} V_{P0\mathrm{sat}}^2}{\rho_{\mathrm{sat}} V_{P0\mathrm{sat}}^2 - K_{P0}} + \frac{K_P - K_{P0}}{\rho_{\mathrm{sat}} V_{P0\mathrm{sat}}^2 - K_{P0}} \tag{20}$$

where $V_{P0\mathrm{sat}}$ is the wet-rock P-wave velocity at the undamaged state.

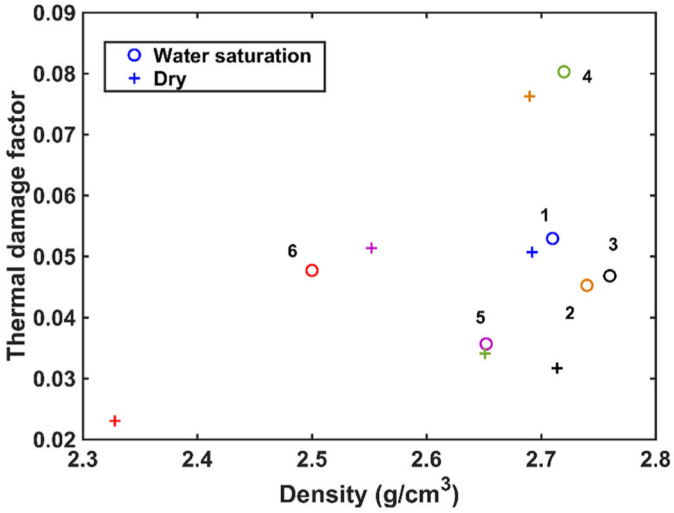

Figure 7. TDF as a function of density at water-saturation and dry conditions.

4. Results

4.1 P-wave velocity variation rate and thermal damage

The P-wave velocities are measured before and after heating, and the P-wave velocity variation rate is defined as

$$\Delta V = \frac{V_{P0} - V_{PT}}{V_{P0}}. \tag{21}$$

Figure 5 shows the P-wave velocity variation rate as a function of temperature at water-saturation and dry conditions. Increasing temperature, the rate increases steadily, indicating that rock damage gradually begins. Heating the rock leads to opening of microcracks [46]. According to Figure 5a and b, when the porosity and permeability of rock are relatively large, the velocity variation rate of the water-saturated rock is higher than that of the dry rock (sample 6), indicating that with the increase of temperature, the fluid affects the degree of damage, so that the effect of temperature on the fluid properties cannot be neglected [45]. The velocity variation rate of the six samples exhibits no direct relation with porosity.

Figure 6 shows the TDFs computed from Equation (6), indicating that it increases with temperature. The damage factors are small in the temperature range, less than 0.1. This is due to the fact that the decrease of pore volume caused by the mineral expansion is greater than the pore volume increase caused by free water loss. Then, the sample is relatively dense at the macroscale [19]. When the temperature is lower than 70 °C, the TDF is negative. Figure 6c shows negative values at dry conditions, an abnormal situation [22]. At the same temperature, when the porosity and permeability are relatively large, the TDF of the water-saturated sample is higher than that of the dry one (see Figure 6c and f).

4.2. Effect of density, porosity and permeability

Figure 7 shows the TDF as a function of the density at 130 °C at water-saturation and dry conditions. For sample 1 (also see Figure 6a), the difference between the two conditions is 0.018 g/cm^3, but it decreases as the temperature increases. For the other samples the difference is higher, and

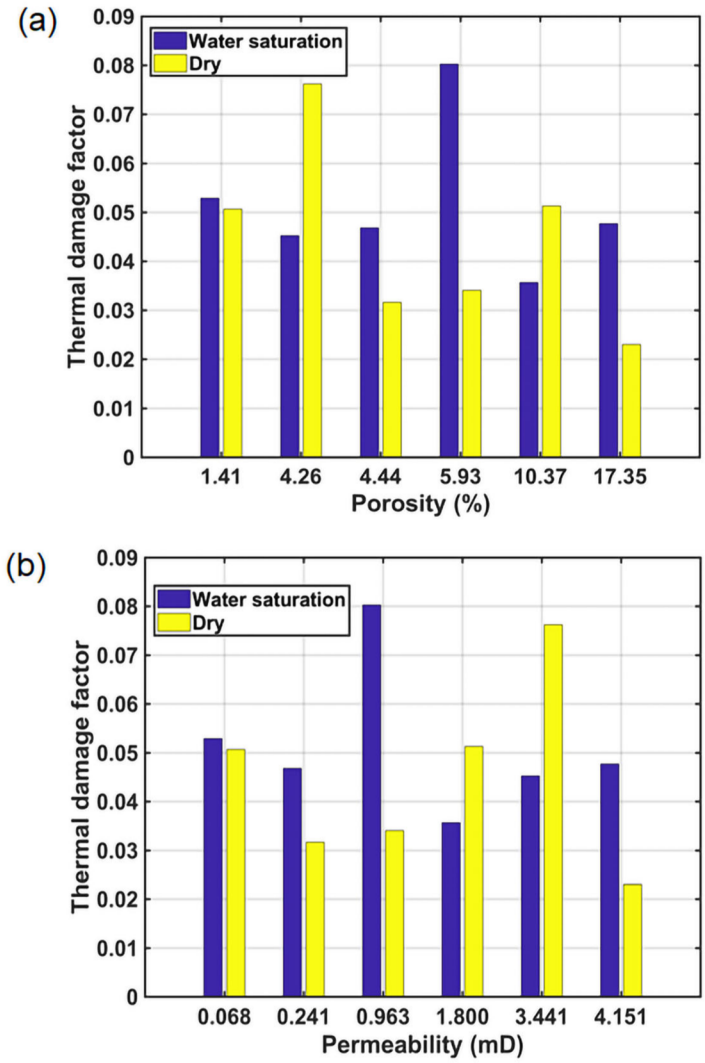

Figure 8. TDF as a function of porosity (a) and permeability (b) at water-saturation and dry conditions.

with the increase of temperature, it increases significantly. In general, there is a linear relation between density and TDF.

The pore space morphology, porosity and permeability change with heating. Some rocks are less sensitive and require very high temperatures (above 400 °C) to exhibit a significant increase in permeability [47]. We consider up to 130 °C, and the permeability and porosity are basically constant (see Figure 8), but the wet and dry cases show significant differences.

4.3. Effect of the microcrack properties

The development of microcracks indicates that the rock is being damaged. The microcrack porosity is estimated by using the aforementioned rock model. Figure 9 shows the effect of microcrack density, porosity and aspect ratio on the TDF in samples at 130 °C. Microcrack density and

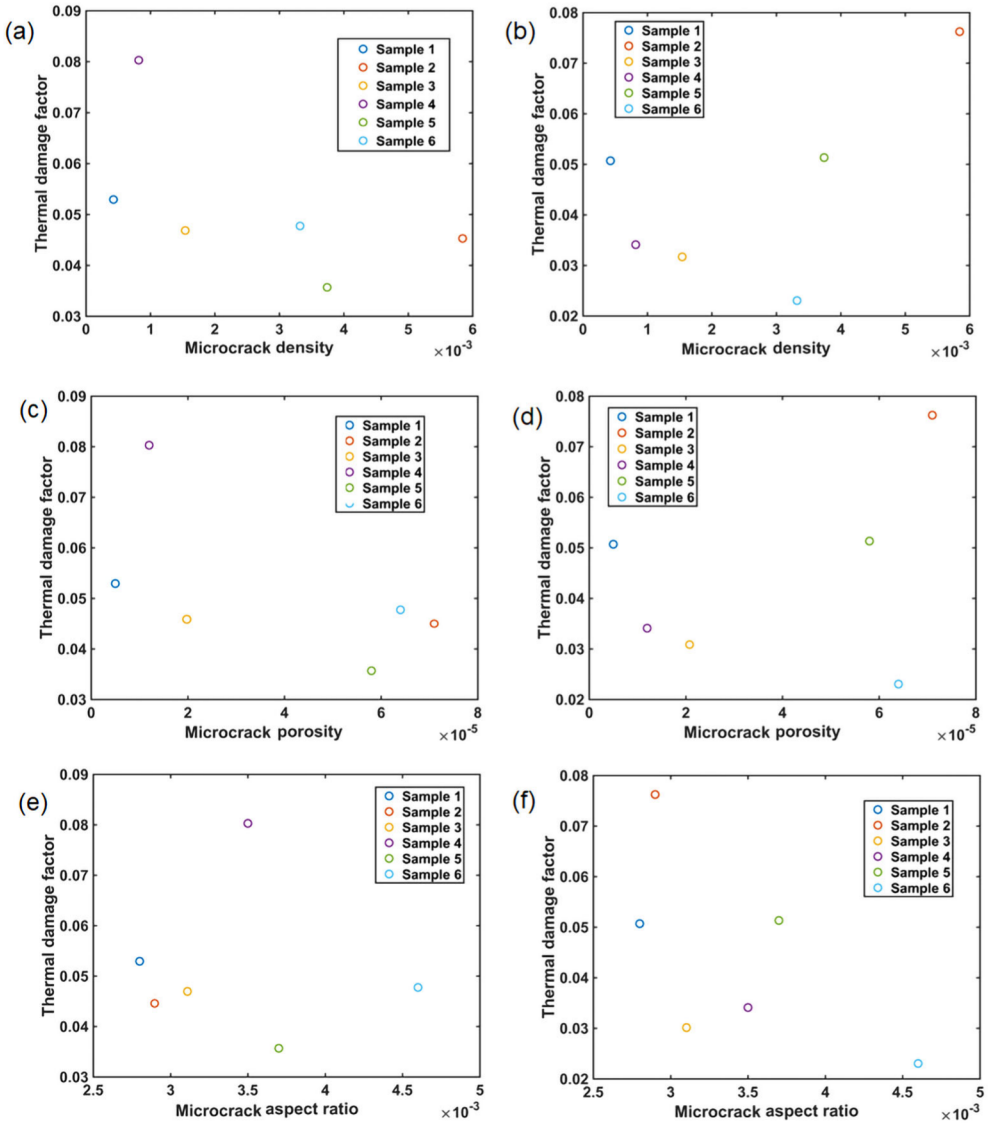

Figure 9. TDF as a function of microcrack density (a, b), microcrack porosity (c, d) and microcrack aspect ratio (e, f) at water-saturation (a, c, e) and dry (b, d, f) conditions.

porosity exhibit the same trend with respect to the TDF. For aspect ratios, the TDF is large, indicating that the rock is easier to deform.

4.4. Effect of the critical temperature of microcrack propagation

We compute the critical temperature corresponding to the irreversibility threshold of microcrack propagation. Figure 10 shows the results at full water saturation, where the critical temperature is indicated. It shows that the aspect ratio decreases with temperature. For high porosity, the microcrack aspect ratio is high and the critical temperature is low. With a lower critical temperature, the rock is more likely to be damaged thermally in the high temperature range.

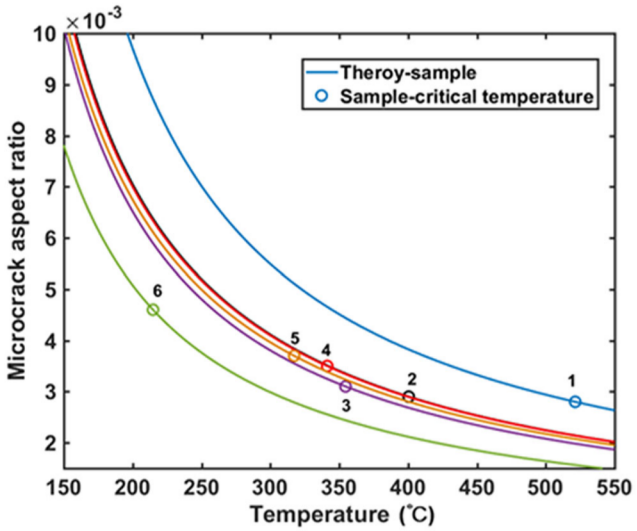

Figure 10. Critical temperature corresponding to the threshold of irreversibility of microcrack propagation at full water saturation.

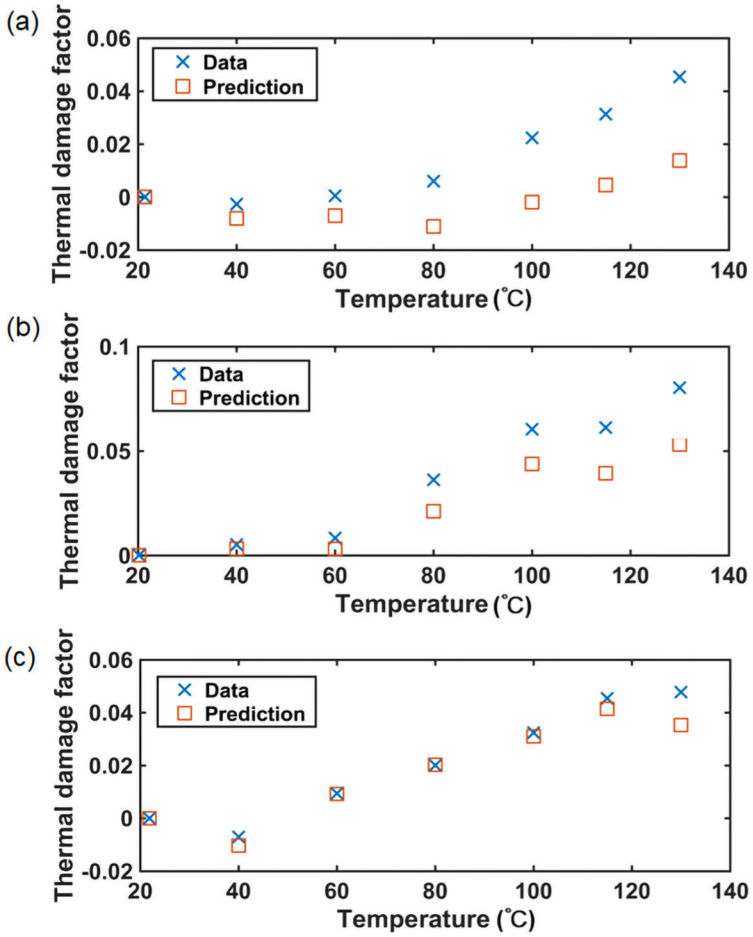

Figure 11. Estimated and actual results of the TDFs of water-saturated samples 2 (a), 4 (b) and 6 (c), at different temperatures.

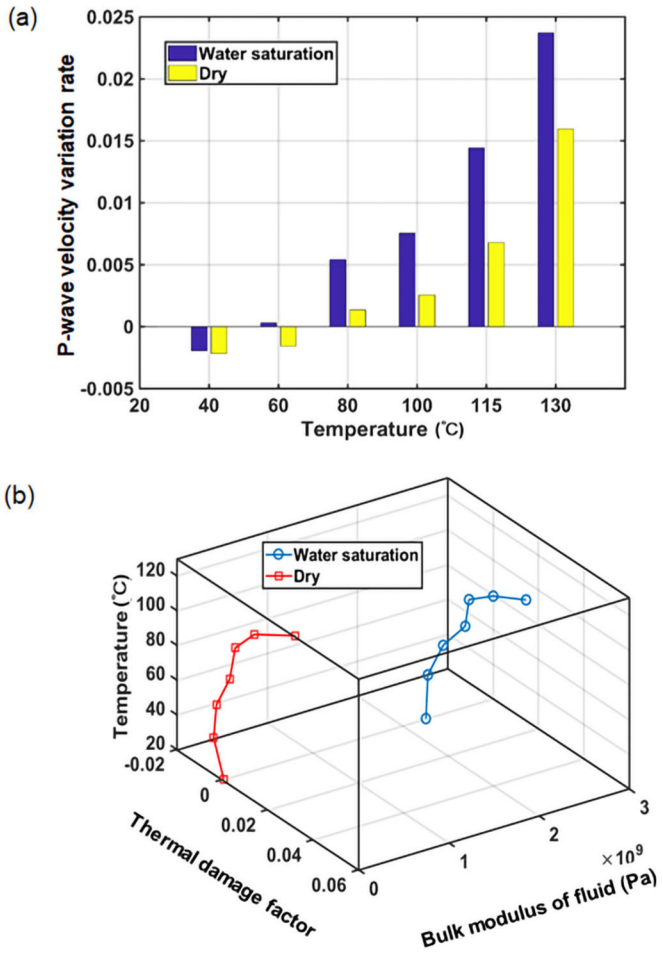

Figure 12. P-wave velocity variation rate with temperature at saturated and dry conditions (a) and relation between the TDF and fluid bulk modulus varying with temperature (b).

4.5. Effect of the fluid

4.5.1. Estimating the TDF of saturated rocks

We assume that the dry-rock TDF is known, and the wet-rock one is estimated by fluid substitution using the Gassmann equation (see Equations (6) and (14)–(19)). We select three samples. Figure 11 compares the predicted and measured values in water-saturated samples 2, 4 and 6, at different temperatures. The estimations are in good agreement with the actual values at low temperatures, indicating that the proposed method can effectively describe the variation of the TDF in that range. The TDFs increase with increasing temperature and the thermal expansion results in volume variations [29, 48]. In this case, thermal stress effects occur within and between grains due to the different thermal expansion rates between minerals and fluids. When the temperature rises to a certain extent, the thermal stress inside exceeds the tensile yield of the grain contacts, and the rock internal structure is damaged, leading to the development of new microcracks.

4.5.2. Difference in TDF between dry and saturated rocks

Figure 11 shows that when temperature increases, the TDF of the saturated rock is underestimated and the difference between the saturated and dry ones increases. The variation of the fluid bulk modulus leads to

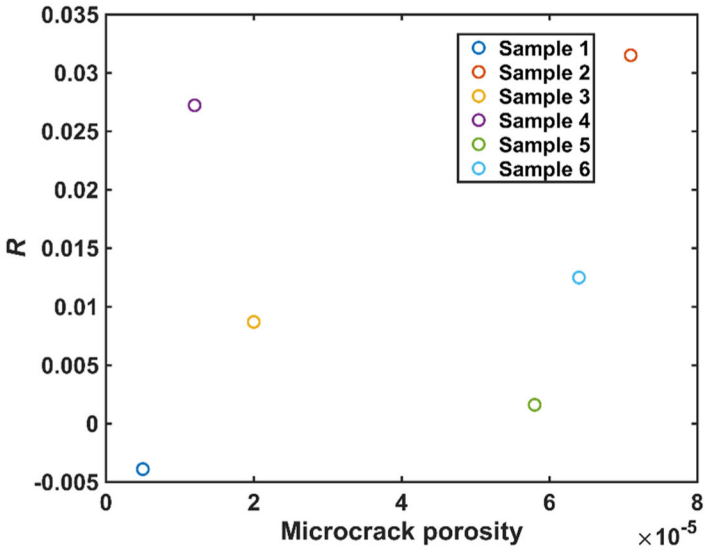

Figure 13. *R* as a function of microcrack porosity at 130 °C.

variations of the wet-rock modulus and thermal damage occurs. Taking sample 2 as an example and the same temperature difference, as shown in Figure 12a, the P-wave velocity at the dry condition varies less than that of the saturated sample. When the rock is water saturated, the effective bulk and shear moduli increase and are positively correlated with the P-wave velocity. Figure 12b shows the relation between the TDF and the fluid bulk modulus. With the increase of temperature, the moduli of water and gas decrease and TDF increases, indicating that the contribution of the fluid cannot be neglected.

As shown in Figure 11, there is a significant difference between the measured and predicted TDF at high temperatures. We define this difference as $R = D_M - D_P$, where D_M and D_P the actual and theoretical values, respectively. Figure 13 shows that R increases as a function of the microcrack porosity (temperature is 130 °C). Heated water affects the rock skeleton, thus affecting the thermal damage of the rock.

5. Conclusion

We have measured the ultrasonic velocity of six saturated/dry carbonate samples as a function of temperature and analyzed the thermal damage. At the same temperature, when the porosity and permeability of the rock are relatively large, the TDF of the saturated rock is higher than that of the dry rock, indicating that the presence of fluids has an important effect.

The thermal-damage model combined with the Gassmann equation are used to estimate the wet-rock TDF. The difference between TDFs in the wet and dry cases increases with the bulk density difference. If the rock porosity and permeability are low, this difference is small, while at the same temperature and increasing permeability, the difference is significant. The higher the microcrack aspect ratio is, the lower the critical temperature corresponding to the irreversibility threshold of microcrack propagation is, and the rock is more likely to suffer damage at high temperatures. In the high temperature range, the theory underestimates the actual values. Basically, the TDF is affected by the properties of the microcracks and fluid type.

Funding

This work is supported by the National Natural Science Foundation of China (grant no. 41974123 and 42174161), and the Jiangsu Province Science Fund for Distinguished Young Scholars (grant no. BK20200021).

References

[1] B. Danial, A. Kaveh, and M. S. Rahim, "Modeling of shear wave velocity in limestone by soft computing methods," *Int. J. Mining Sci. Technology*, vol. 27, no. 3, pp. 423–430, 2017.

[2] J. Sundberg, P. E. Back, R. Christiansson, M. Hökmark, M. Ländell, and J. Wrafter, "Modelling of thermal rock mass properties at the potential sites of a Swedish nuclear waste repository," *Int. J. Rock Mechanics Mining Sciences*, vol. 46, no. 6, pp. 1042–1054, 2009. DOI: 10.1016/j.ijrmms.2009.02.004.

[3] Z. Zeng, X. Chen, J. Li, T.-l Li, and L. H. Zhang, "Advancement of geothermal geophysics exploration," *Progress Geophys.*, vol. 27, no. 1, pp. 168–178, 2012.

[4] L. H. Kristinsdóttir *et al.*, "Electrical conductivity and P-wave velocity in rock samples from high-temperature Icelandic geothermal fields," *Geothermics*, vol. 39, no. 1, pp. 94–105, 2010. DOI: 10.1016/j.geothermics.2009.12.001.

[5] S. Chaki, M. Takarli, and W. P. Agbodjan, "Influence of thermal damage on physical properties of a granite rock: Porosity, permeability and ultrasonic wave evolutions," *Constr. Build. Mater.*, vol. 22, no. 7, pp. 1456–1461, 2008. DOI: 10.1016/j.conbuildmat.2007.04.002.

[6] Z. K. Crosby, P. M. Gullett, S. A. Akers, and S. S. Graham, "Characterization of the mechanical behavior of salem limestone containing thermally-induced microcracks," *Int. J. Rock Mech. Mining Sci.*, vol. 101, pp. 54–62, 2018. DOI: 10.1016/j.ijrmms.2017.11.002.

[7] F. Bouchaala *et al.*, "Scattering and intrinsic attenuation as a potential tool for study of a fractured reservoir," *J. Petroleum Sci. Eng.*, vol. 174, pp. 533–543, 2019. DOI: 10.1016/j.petrol.2018.11.058.

[8] M. Chapman, "Frequency-dependent anisotropy due to meso-scale fractures in the presence of equant porosity," *Geophys. Prospecting*, vol. 51, no. 5, pp. 369–379, 2003. DOI: 10.1046/j.1365-2478.2003.00384.x.

[9] L. Kong, B. Gurevich, Y. Zhang, and Y. Wang, "Effect of fracture fill on frequency-dependent anisotropy of fractured porous rocks," *Geophys. Prospecting*, vol. 65, no. 6, pp. 1649–1661, 2017. DOI: 10.1111/1365-2478.12505.

[10] P. Tillotson, M. Chapman, J. Sothcott, A. I. Best, and X. Y. Li, "Pore fluid viscosity effects on P- and S-wave anisotropy in synthetic silica cemented sandstone with aligned fractures," *Geophys. Prospecting*, vol. 62, no. 6, pp. 1238–1252, 2014. DOI: 10.1111/1365-2478.12194.

[11] C. David, B. Menendez, and M. Darot, "Influence of stress-induced and thermal cracking on physical properties and microstructure of La Peyratte granite," *Int. J. Rock Mech. Mining Sci.*, vol. 36, no. 4, pp. 433–448, 1999. DOI: 10.1016/S0148-9062(99)00010-8.

[12] A. Hassanzadegan, G. Blöcher, H. Milsch, L. Urpi, and G. Zimmermann, "The effects of temperature and pressure on the porosity evolution of flechtinger sandstone," *Rock Mech. Rock Eng.*, vol. 47, no. 2, pp. 421–434, 2014. DOI: 10.1007/s00603-013-0401-z.

[13] H. Tian, T. Kempka, N. X. Xu, and M. Ziegler, "Physical properties of sandstones after high temperature treatment," *Rock Mech Rock Eng.*, vol. 45, no. 6, pp. 1113–1117, 2012. DOI: 10.1007/s00603-012-0228-z.

[14] H. Yavuz, S. Demirdag, and S. Caran, "Thermal effect on the physical properties of carbonate rocks," *Int. J. Rock Mech. Mining Sci.*, vol. 47, no. 1, pp. 94–103, 2010. DOI: 10.1016/j.ijrmms.2009.09.014.

[15] W. Zhang, Q. Sun, S. Zhu, and B. Wang, "Experimental study on mechanical and porous characteristics of limestone affected by high temperature," *Appl. Thermal Eng.*, vol. 110, pp. 356–362, 2017. DOI: 10.1016/j.applthermaleng.2016.08.194.

[16] J. W. Dougill, J. C. Lau, and N. J. Burt, 1977, "Toward a Theoretical Model for Progressive Failure and Softening in Rock," *Concrete and Similar Material*. Waterloo: University of Waterloo Press.

[17] T. Hueckel, A. Peano, and R. Pellegrini, "A thermo-plastic constitutive law for brittle-plastic behavior of rocks at high temperatures," *PAGEOPH*, vol. 143, no. 1–3, pp. 483–510, 1994. DOI: 10.1007/BF00874339.

[18] N. N. Sirdesai, A. Singh, L. K. Sharma, R. Singh, and T. N. Singh, "Determination of thermal damage in rock specimen using intelligent techniques," *Eng. Geol.*, vol. 239, no. 9, pp. 179–194, 2018. DOI: 10.1016/j.enggeo.2018.03.027.

[19] H. Sun, Q. Sun, W. N. Deng, W. Q. Zhang, and L. Chao, "Temperature effect on microstructure and P-wave propagation in linyi sandstone," *Appl. Thermal Eng.*, vol. 115, pp. 913–922, 2017. DOI: 10.1016/j.applthermaleng.2017.01.026.

[20] J. Yang, L.-Y. Fu, W. Zhang, and Z. Wang, "Mechanical property and thermal damage factor of limestone at high temperature," *Int. J. Rock Mech. Mining Sci.*, vol. 117, pp. 11–19, 2019. DOI: 10.1016/j.ijrmms.2019.03.012.

[21] M. Yao, G. Rong, C. Zhou, and J. Peng, "Effects of thermal damage and confining pressure on the mechanical properties of coarse marble," *Rock Mech. Rock Eng.*, vol. 49, no. 6, pp. 2043–2054, 2016. DOI: 10.1007/s00603-016-0916-1.

[22] W. Zhang, Q. Sun, S. Hao, and B. Wang, "Experimental study on the thermal damage characteristics of limestone and underlying mechanism," *Rock Mech. Rock Eng.*, vol. 49, no. 8, pp. 2999–3008, 2016. DOI: 10.1007/s00603-016-0983-3.

[23] M. Batzle, R. Hofmann, and D. H. Han, "Heavy Oils— Seismic Properties: The Leading Edge," vol. 25, no. 6, pp. 750–757, 2006. DOI: 10.1190/1.2210074.

[24] A. Rabbani, D. R. Schmitt, J. Nycz, and K. Gray, "Pressure and temperature dependence of acoustic wave speeds in bitumen saturated carbonates: Implications for seismic monitoring of the Grosmont Formation," *Geophysics*, vol. 82, no. 5, pp. MR133–MR151, 2017. DOI: 10.1190/geo2016-0667.1.
[25] M. Grab, B. Quintal, E. Caspari, C. Deuber, H. Maurer, and S. Greenhalgh, "The effect of boiling on seismic properties of water-saturated fractured rock," *J. Geophys. Res. Solid Earth*, vol. 122, no. 11, pp. 9228–9252, 2017. DOI: 10.1002/2017JB014608.
[26] M. S. Jaya, S. A. Shapiro, L. H. Kristinsdóttir, D. Bruhn, H. Milsch, and E. Spangenberg, "Temperature dependence of seismic properties in geothermal rocks at reservoir conditions," *Geothermics*, vol. 39, no. 1, pp. 115–123, 2010. DOI: 10.1016/j.geothermics.2009.12.002.
[27] D. Xi, X. Liu, and C. Zhang, "The frequency (or time) - temperature equivalence of relaxation in saturated rocks," *Pure Appl. Geophys.*, vol. 164, no. 11, pp. 2157–2173, 2007. DOI: 10.1007/s00024-007-0270-z.
[28] A. M. Ferrero and P. Marini, "Experimental studies on the mechanical behaviour of two thermal cracked marbles," *Rock Mech. Rock Eng.*, vol. 34, no. 1, pp. 57–66, 2001. DOI: 10.1007/s006030170026.
[29] J. T. Fredrich and T. Wong, "Micromechanics of thermally induced cracking in three crustal rocks," *J. Geophys. Res.*, vol. 91, no. B12, pp. 743–764, 1986.
[30] M. Keshavarz, F. L. Pellet, and B. Loret, "Damage and changes in mechanical properties of a gabbro thermally loaded up to 1,000 °C," *Pure Appl. Geophys.*, vol. 167, no. 12, pp. 1511–1523, 2010. DOI: 10.1007/s00024-010-0130-0.
[31] W. Lin, "Permanent strain of thermal expansion and thermally induced microcracking in Inada granite," *J. Geophys. Res.*, vol. 107, no. B10, pp. 2215, 2002.
[32] M. L. Ravalec and Y. Guéguen, Permeability models of heated saturated igneous rocks. *J. Geophys. Res.*, vol. 99, no. B12, pp. 251–324, 1994.
[33] E. C. David and R. W. Zimmerman, "Pore structure model for elastic wave velocities in fluid-saturated sandstones," *J. Geophys. Res.*, vol. 117, no. B7, pp. n/a–n/a, 2012. DOI: 10.1029/2012JB009195.
[34] F. Gassmann, "Über Die Elastizität Poröser Medien," *Vierteljahrsschrift der Naturforschenden Gesselschaft in Zürich*, vol. 96, pp. 1–23, 1951.
[35] W. F. Murphy, L. M. Schwartz, and B. Hornby, "Interpretation physics of VP and VS in sedimentary rocks," Paper presented at the SPWLA 32nd Annual Logging Symposium, Midland, Texas, June, pp. 1–24, 1991.
[36] A. B. Stevens, "A new device for determining porosity by the gas-expansion method," *Petroleum Technol.*, vol. 2, no. 02, pp. 1–5, 1939. DOI: 10.2118/939054-G.
[37] R. P. Ma and J. Ba, "Coda and intrinsic attenuations from ultrasonic measurements in tight siltstones," *J. Geophys. Res.: Solid Earth*, vol. 125, no. 4, pp. 125, 2020.
[38] H. B. Zhao, G. Z. Yin and L. J. Chen, "Experimental study on effect of temperature on sandstone damage," *Chinese J. Rock Mechanics Engineering*, vol. 28, no. s1, pp. 2784–2788, 2009.
[39] L. M. Kachanov, *Introduction to Continuum Damage Mechanics*, Dordrecht: Springer, 1986.
[40] S. Zhu, W. Zhang, Q. Sun, S. Deng, J. Geng, and C. Li, "Thermally induced variation of primary wave velocity in granite from Yantai: Experimental and modeling results," *Int. J. Therm. Sci.*, vol. 114, pp. 320–326, 2017. DOI: 10.1016/j.ijthermalsci.2017.01.008.
[41] B. R. Lawn, *Fracture of Brittle Solids*, New York: Cambridge University Press, 1993.
[42] L. Vernik and M. Kachanov, "Modeling elastic properties of siliciclastic rocks," *Geophysics*, vol. 75, no. 6, pp. E171–E182, 2010. DOI: 10.1190/1.3494031.
[43] T. Mori and K. Tanaka, "Average stress in matrix and average elastic energy of materials with misfitting inclusions," *Acta Metall.*, vol. 21, no. 5, pp. 571–574, 1973. DOI: 10.1016/0001-6160(73)90064-3.
[44] R. W. Zimmerman, *Compressibility of Sandstones*. Amsterdam: Elsevier, 1991.
[45] M. L. Batzle and Z. Wang, "Seismic properties of pore fluids," *Geophysics*, vol. 57, no. 11, pp. 1396–1408, 1992. DOI: 10.1190/1.1443207.
[46] Z. K. Zhao, Q. Z. Sun, P. Q. Zhang, H. O. Jing, and Y. M. Sun, "Phase transformation and expansibility of quartz sands during heating," *J. Mater. Eng.*, vol. 28, no. 10, pp. 25–27, 2006.
[47] W. H. Somerton, *Thermal Properties and Temperature-Related Behavior of Rock/Fluid Systems*. United States: Elsevier, 1992.
[48] L. Pimienta, L. F. Orellana, and M. Violay, "Variations in elastic and electrical properties of crustal rocks with varying degree of microfracturation," *J. Geophys. Res. Solid Earth*, vol. 124, no. 7, pp. 6376–6396, 2019. DOI: 10.1029/2019JB017339.